INTEGRATED GEOCHEMICAL AND GEOPHYSICAL CHARACTERISATION OF TOURMALINE-BEARING PEGMATITES FROM IJERO-EKITI, SOUTHWESTERN NIGERIA

R. O. JIMOH, O. OLOGE, A. O. AFOLABI*, J. AJADI & B. R. ONAWOLA

R. O. J.: Departmentt of Chemical and Geological Sciences, Al-Hikmah University, P. M. B. 1601, Ilorin, Nigeria; O. O.: Department of Geophysics, Federal University, Birnin Kebbi, Nigeria; A. O. A.: Department of Earth Sciences, Ladoke Akintola University of Technology, Ogbomoso, Nigeria; J. A.: Department of Geology and Mineral Science, Kwara State University, Ilorin, Nigeria; B. R. O.: Department of Physics, University of Ibadan, Nigeria.

**Corresponding author's: oaafolabi@lautech.edu.ng*

ABSTRACT

The Ijero-Ekiti tourmaline-bearing pegmatite was investigated, using geological, geochemical, and geophysical methods to characterize its geological evolution and evaluate its mineralisation potential. Petrographical studies revealed a typical granitic mineralogical composition of quartz, feldspar, and muscovite, with tourmaline as accessory minerals. Geochemical data on whole rock analysis showed high and moderate enrichments in SiO_2 (av. 71.65 wt. %) and Al_2O_3 (av. 14.71 wt. %) respectively, while mean values for the other major oxides ranged between 0.01 and 3.63 wt. %. Results also showed that K_2O (av. 3.63 wt. %) and Na_2O (av. 3.52 wt. %) concentrations were comparable to average Upper Continental values. The relatively high aluminum and alkaline compositions could be attributed to pneumatolytic crystallization from the pegmatitic melt. Aluminum Saturation Index (ASI) [Al/(Ca+Na+K)] indicated peraluminous character. Ranges of some trace elements (Cs, 1.5 – 705.6 ppm; Be, 0.5 – 12 ppm; Sn, 2.0 – 34 ppm; Ta, 1.0 – 14) support a Lithium-Cesium-Tantalum (LCT) type rare-elements pegmatites for the pegmatites of the study. The spider and K/Rb vs K/Cs plots portrayed fractionation trends suggestive of potential mineralisation. The vertical electric sounding data showed that pegmatites underlie the lateritic zone and represent the anomalous layer characterized by high resistivity values ranging from 1086 to 9489 Ohm-m with the surface to a maximum depth of 20.8m which is suspected to be a mineralised zone. Some of these pegmatites are highly tourmalinated, suggesting that they emanate from highly mineralised magma and are believed to represent late-stage pneumatolytic fluids derived from acidic magma bodies through magmatogenic processes.

Keyword: Mineralisation, Pegmatite, Magma, Pneumatolytic, High-resistivity

Introduction

Tourmaline, a group of boron aluminum cyclosilicate mineral, with a typical complex chemical formula $Na(Mg,Fe)_3Al_6(BO_3)_3(Si_6O_{18})(OH)_4$ is a semi-precious gem mineral with variable colours and physical properties making them suitable for adornment and decorative purposes. Gem mineralisations across southwestern Nigeria, including tourmaline occurrences in Ijero-Ekiti

are essentially pegmatitic, mainly involving multiple magmatic processes with diverse sets of structurally controlled discrete episodes of mineralisation, with incontrovertible evidence from crosscutting relationships (Jimoh, 2018). Rare-element pegmatites are very important resources for economic concentrations of high-quality gem and industrial minerals, including tourmaline. Gem quality tourmalines crystallize almost exclusively from rare-elements and in miarolitic class, lithium-cesium-tantalum (LCT)-family pegmatites (Olatunji & Jimoh, 2017). LCT-granitic pegmatites as defined by Černý (1991b) are anomalously enriched in Li, Rb, Cs, Be, B, Sn, Ga, Ta, Nb and F and are hosts to many of the world's most precious gemstones including gem tourmaline and beryl. Studies have revealed that a number of tourmaline species such as schorl, elbaite, liddicoatite, magnesiofoitite, rossmanite and olenite occur in these types of pegmatites (Hawthorne *et al*., 1993; Selway *et al*., 1998). Ijero-Ekiti pegmatites are rare metals granitic pegmatites that are widely distributed with a marked concentration of mineralised pegmatites in a broad belt, a pegmatite field believed to be part of the late Pan African orogeny (Wright, 1970, Olisa *et al.*, 2018). Rare-metal mineralisation is particularly and genetically associated with post orogenic geochemically distinctive granitoids (Tischendorf, 1977; London, 1996). Rare element concentrations in pegmatites of granitic compositions are considered to be a vital tool in contrasting genetic models either as magmatogenic (Ginsburg *et al.*, 1979; Černý, 1989a; Bradley *et al.*, 2017) or metamorphic anatectic bodies (Sokolov, 1981; Shaw, *et al.*, 2016; Sweetapple, 2017; Duuring, 2020; Xuanchi, *et al.*, 2024).

The demand for rare metals and gemstones has increased globally and created the need for renewed search for economically viable deposits (Okunlola & Oyedokun, 2009). Direct detection of a mineralised environment may depend on any one or a combination of density, magnetism, radioactivity, geochemical and electrical properties (Dentith & Mudge, 2014). Internal distribution of physical properties of the subsurface or near the earth's surface greatly influence results from any geophysical measurements. Analysis of these measurements can reveal how the physical properties of the subsurface vary. Solid mineral exploration requires integration and interpretation of geochemical and high-resolution geophysical data which are usually targeted at delineating possible host rocks' characteristics and structures (Amigun & Anu, 2013). In the exploration for subsurface resources, methods used are capable of detecting and delineating local features of economic interest that could not be discovered by any realistic drilling programme (Kearey *et al.*, 2002), hence the need for this research. Ijero-Ekiti and environ lies within the southwestern Nigeria Basement Complex, between latitudes 7^0 48' 36" to 7^0 50' 06" and longitudes 5^0 03' 54" to 5^0 05' 42", and underlain by migmatitic gneiss which are overlain by sheared narrow quartzite ridges in close association with undifferentiated schist serving host to several pegmatite intrusions. An integrated study on the Ijero pegmatite was carried out based on whole rock geochemical analysis of tourmaline-bearing pegmatites and geophysical data to characterize the geological evolution and mineralisation potentials of the pegmatites.

\

Experimental

Geochemical methods

Ijero-Ekiti and environs were systematically mapped to ascertain rock types and their relationships. Fresh samples of the tourmaline-bearing pegmatites in the area were collected for both petrographical and geochemical studies. Thirteen of such samples were pulverized and analyzed for their major and trace elements compositions at the ACME Laboratories, Vancouver, Canada, using the Inductively Coupled Plasma Mass Spectroscopy (ICP-MS) technique after fusion with $LiBO_2$. 0.2gm of the powdered samples and 1.5gm of $LiBO_2$ flux were mixed in a graphite crucible and heated to $1{,}050^0$C for 15 min. The molten samples were then digested in strong and hot acid ranging from simple nitric acid to hydrofluoric acid. The aqueous samples were converted to aerosols via a nebuliser and then transported to the inductively coupled plasma which is a high temperature zone (8,000–10,000ºC). The analytes were heated (excited) to the respective ions. While in a quadrupole mass filter, these ions were separated based on their mass-to- charge ratios and the ion intensities at different masses measured (mass spectrometry). These ion intensities are proportional to the respective concentrations of analytes in the aqueous sample. The detection limit for major oxides is 0.1%, while that of the trace elements ranged from 0.01 to 1ppm. The quantification is an external multi-point linear calibration by comparing the ion intensity of an unknown sample with that of a standard sample. Multi-element calibration standard solutions were prepared from single- and multi element primary and/or in-house working standard solutions. Rhodium (Rh) was used as an internal reference standard.

Geophysical technique

A total of ten sampled vertical electrical sounding (VES) points were located randomly within the study area. Data acquisition was done using the Abem SAS 4000 terrameter, Schlumberger electrical resistivity configuration was employed with a maximum of half electrode spacing AB/2 of 100 m and a maximum electrode potential separation of MN/2 which was kept constant. The array is capable of isolating successive overlap in the resistivity of different rock layers beneath the surface using their resistivity contrast (Mosuro *et al.*, 2011). The potential electrode separation was kept constant as a result of the shallow nature of the area basement rock and the current electrodes were progressively moved outward symmetrically about the centre of the configuration. This measured resistance (R) was multiplied by the corresponding Geometric Factor (a function of the electrode spacing and configuration) to obtain the apparent resistivity measured in Ohmmeter (Ωm) needed for the interpretation. Qualitative and quantitative interpretation of data was done using 'Winresist' (a computer software package). The sounding curves for each point were obtained by plotting the apparent resistivity against the current electrode spacing/distance (AB/2) on a log – log graph, the apparent resistivity on the ordinate axis and the electrode spacing AB/2 on the abscissa axis and automatically generated the number of rock layers corresponding to their mineralogical compositions. The plot obtained from the software was examined, the plot form and character of each VES point was noted in terms of resistivity variation with depth. The curve types with their corresponding thickness were noted which form parts of the parameters used for analysis.

Geological setting

Ijero-Ekiti is underlain by crystalline rocks of the Nigerian Basement Complex, a Pan-African mobile belt that lies between the West African and Congo Cratons, and (Black, 1980, Adetunji, *et al.*, 2018; Tijani, 2023). It is a polycyclic terrain which suffered its most pronounced deformation and mobilization during the Pan-African age (600 Ma). Different ages have been ascribed to the Nigerian Basement Complex rocks using different radiometric dating methods such as Rb/Sr, K/Ar and Th/Pb (Tubosun *et al.*, 1984). Grant, (1970) observed that majority of the radiometric ages obtained fall in the range of 600 Ma, which corresponds to the Pan-African thermo-tectonic event. The Basement Complex, which is Precambrian in age, is made up of the Migmatite-Gneiss Complex, the Schist Belts and the Older Granites (Fig. 1). The Migmatite-Gneiss which is the most widespread making up about 60% of the surface area of the Nigerian Basement Complex (Rahaman & Ocan, 1978; Oyinloye, 2011, Elatikpo *et al.*, 2013), has a heterogeneous assemblage comprising; migmatites, orthogneiss, paragneiss, granite-gneiss and a series of basic and ultrabasic metamorphosed rocks. The Schist Belt is a north-south trending supracrustal assemblage of low to medium grade metasedimentary rocks with subordinate mafic and ultramafic rocks, consisting of quartzites, amphibolite, mica-schist, calc-silicate rocks, marbles, phyllites, pelites, meta-conglomerate iron formations and subordinate meta-igneous rocks (Elueze, 1992). The Older Granites, occurring intricately with the Migmatite-Gneiss Complex and the infolded Schist Belts as intrusives, are believed to have been emplaced during the Pan-African orogeny (Harper *et al.*, 1973). Much of the migmatisation of the Gneiss Complex is believed to have taken place during the later stages of Older Granite activity. However, evidence suggests that by the time intrusive activity started, the Gneiss Complex was already composed of extensively metamorphosed rock groups.

The Pan-African intrusive suite comprises mainly calc-alkaline suites of granites and granodiorite, with subordinate pegmatite and Aplites (Adetunji & Ocan, 2010). Affiliated rocks include charnockites, syenites, tonalites, adamellites, quartz monzonites and gabbro plus extrusive and hypabyssal bodies, notably dolerite dykes believed to belong to the terminal stage of the Pan-African orogenic event in Nigeria. Results of the rock ages showed that pegmatites' emplacement in southwestern Nigeria occurred mainly after the peak of the Pan-African orogenic event in this area. Ijero-Ekiti rare-elements pegmatites are believed to be part of these pegmatites.

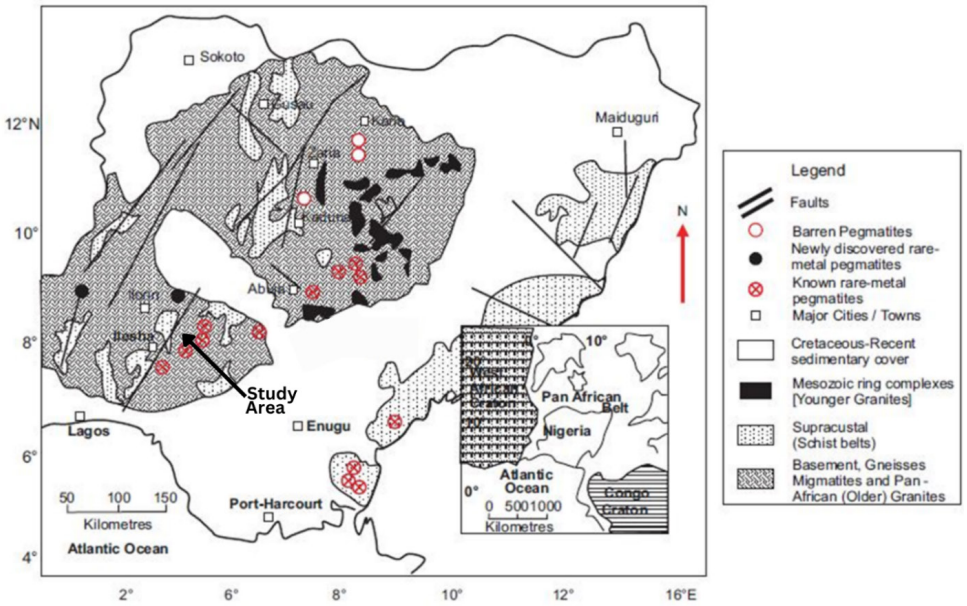

Fig. 1: Geological map of Nigeria showing the regional fractures and location of areas of rare-metal and barren pegmatites (After Garba, 2003).

Lithology, field relationships and petrography of Ijero-Ekiti tourmaline-bearing pegmatites

Ijero-Ekiti and environs are characterized basically by the lithologies of migmatitic gneiss, meta-sedimentary rocks of amphibolite, quartzite, amphibole and biotite schist, and pegmatites (Fig. 2). Though not map-able the amphibole schists, observed to host the pegmatites in the central and western portions of the map area are highly weathered and therefore rarely exposed with only a few bands of the strongly foliated and weathered dark green rock feebly observed along stream channels, road-side cuttings and areas where intensive erosion has occurred. The Ijero metasedimentary rocks have, however, been heavily intruded into by the Pan-African pegmatites, particularly towards the western part of the study area.

The Ijero Pan African pegmatites, some of which are highly mineralised, (Fig. 3) conspicuously occupy the western part of the mapped area. They are very common occurrences within the schist, mostly occurring as large intrusive bodies. In most instances they range in size and shape from small oval intrusions to stocks. The Ijero pegmatites are believed to be part of the mineralised 400km NE-SW-trending pegmatites which belong to the terminal stage of Pan-African magmatism (Rahaman *et al*., 1988; Elueze, 2002). They occur as large bodies that are profusely emplaced within the highly weathered host of amphibolite and amphibole schists covering more than a third of the area. Weathering activities have reshaped the landform of the area. The pegmatites form into hills and valleys

giving rise to the rugged terrain in the area, the schist has been reduced to low-lying plains and most often rarely exposed due to weathering, in the eastern part of the area where biotite schists are exposed and sometimes forming hilly landscape. The widely distributed pegmatites, apart from forming massive and tabular occurrences may also occur as dykes and veins in some few places. Biotite schist represents the major lithology of the Schist Belt. Their occurrences were observed in the central and eastern parts of the study area (Fig. 2), mostly outcropping as low-lying, highly foliated rocks, with characteristic black tints imposed by the preponderance of biotite, and extending southwards. Around Oke-Oro at the northeastern part of the area, outcrops of low-lying migmatite gneiss are observed outcropping particularly along road side cuttings.

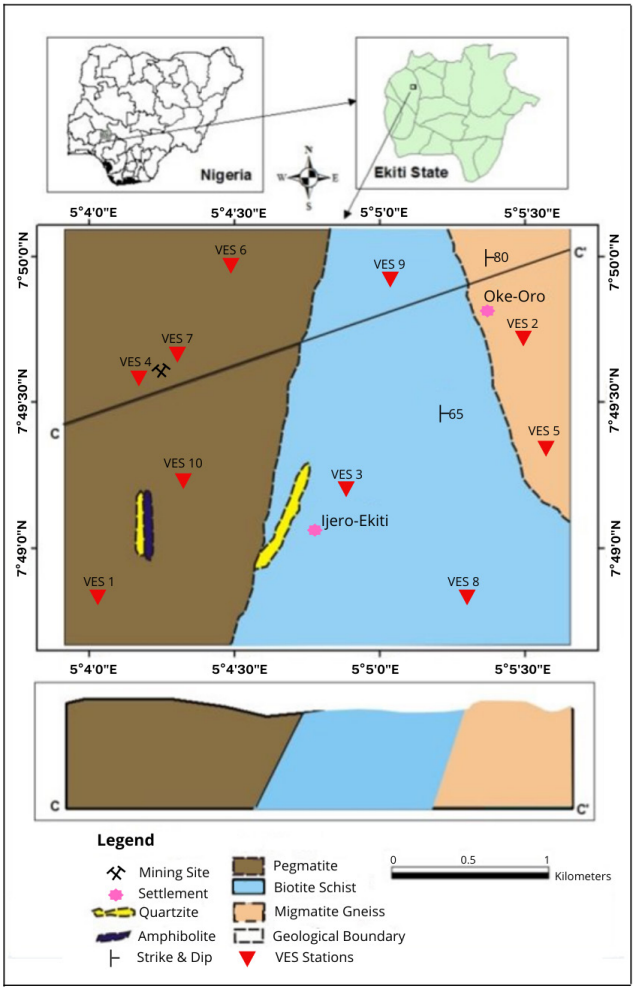

Fig. 2: Geology of Ijero-Ekiti study area.

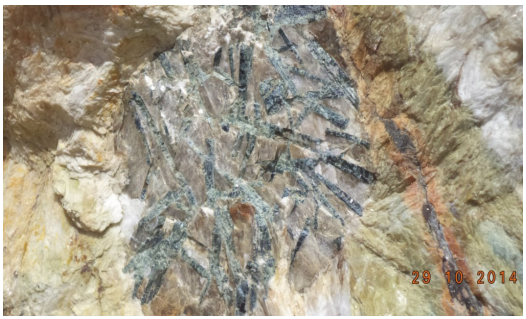

Fig. 3: Euhedral crystals of green tourmaline found associated with quartz and feldspar within the Ijero pegmatite, southwestern Nigeria.

Ijero pegmatites generally occur as coarse-grained rocks with euhedral crystals of quartz, feldspars and bands of muscovite. Lepidolite is also commonly observed in the pegmatite, especially close to its gem-mineralisation. Megascopically, a hand specimen of Ijero pegmatite was observed to consist of large crystals of quartz, K-feldspar, flakes of muscovite and a few thin euhedral crystals of green and black tourmaline as accessory minerals (Fig. 4). Thin section study of the pegmatite reveals a modal composition of K-feldspar (30-35%), quartz (20-25%), muscovite (15-25%), plagioclase (5-10%) and accessory minerals which may include tourmaline, beryl and tantalite-columbite (Fig. 5). Ijero pegmatites' primary mineralisation of tantalum, niobium, tin, beryllium and lithium is hosted in quartz-feldspar-muscovite pegmatites (Kinnaird, 1984). The orthoclase feldspar crystals are found to show some alteration and also exhibit some weak simple twining. Quartz on the other hand was observed with a low positive relief showing some intergrowth with feldspars, which were easily identified with their characteristic twin extinctions and habit. Tourmaline occurs as euhedral to subhedral triangular prismatic crystals showing a range of body colours or colour zoning. Tourmaline's lack of cleavage, high positive relief and strong and intense pleochroism are diagnostic. The tourmaline crystals exhibit long needle-like prismatic shapes with their long axis aligned parallel to each other.

Gem Tourmaline Mineralisation of Ijero-Ekiti tourmaline-bearing pegmatites

Gem mineralisations across southwestern Nigeria, including tourmaline occurrences in Ijero-Ekiti, are essentially within pegmatitic bodies. Euhedral gem quality tourmaline crystals in the granitic pegmatites of the study were found in association with beryl, topaz, spodumene, garnet, cassiterite, tantalite and columbite alongside other rock-forming minerals like quartz, feldspar and muscovite. Crystals of gem tourmaline displaying different colours were found either in miarolitic cavities within the granitic pegmatites or in veins along contacts with their host rocks or are scattered within the body of the pegmatites (Fig. 3). Some tourmaline occurred as giant crystals in the intermediate or core zones of these pegmatites. These large crystals are usually highly fractured and clouded with inclusions, but pegmatite cavities or 'pockets' known as miarolitic cavities provide open spaces into which transparent crystals grow unimpeded, thereby attaining better quality tourmaline crystals with very high degree of internal and external perfection. A great number of such cavities occur within Ijero pegmatites from where several tons of different high-quality tourmaline crystals of varying colours have been evacuated (Fig. 6).

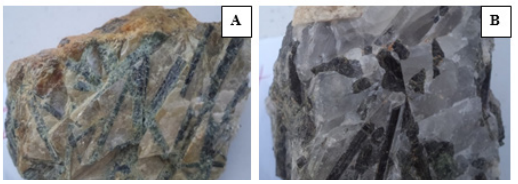

Fig. 4A and B: Hand specimens of Ijero pegmatites containing orthoclase, quartz and tourmaline crystals.

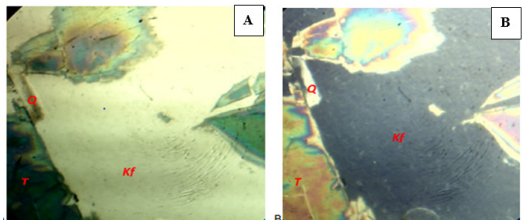

Fig. 5: Photomicrograph of a pegmatite sample from Oke-Kusa mine in Ijero-Ekiti study area, A) under plane polarised light and B) under cross polarised light. Kf = K- feldspar, T = Tourmaline, Q = Quartz (X40).

Fig. 6: A mine excavation within Ijero-Ekiti tourmaline-bearing pegmatites.

Results and Discussions

Geochemical characterisation

The major oxide geochemical data from 13 bulk whole rock samples (Table 1a) of the Ijero-Ekiti tourmaline-bearing pegmatites revealed average SiO_2 and Al_2O_3 values (Table 1b) that are comparable to bulk geochemistry of pegmatites from other places (London, *et al*., 2012; London, 2018). SiO_2 concentrations ranged from 66.41 wt. % to 80.09 wt. % (av. 71.65 wt. %) and Al_2O_3 ranged from 11.82 wt. % to 22.19 wt. % (av. 14.71 wt. %). Adequate concentrations of SiO_2 and Al_2O_3 in a pegmatitic melt are required to provide the silicic and acidic environments necessary for tourmaline crystallisation in pegmatites. The activity of Al_2O_3 or equivalent aqueous species contributes to tourmaline stability and formation, which are favoured in acidic fluids with high availability of Al species (Morgan & London, 1989).

Results showed fair concentrations of the alkali oxides for most of the analysed pegmatite samples mean values of the alkali were 3.52 and 3.63 wt. % respectively for Na_2O and K_2O. These fair concentrations are important as Al transport is facilitated by alkali borate species such as borax, $Na_2B_4O_7$, a mixture of acidic and alkaline boron compound which is essential to provide the necessary Al for tourmaline-forming reactions (Jimoh, 2018). The fairly high mean value of K_2O is necessitated by the high orthoclase content of the pegmatites. Although the mean concentrations for the other major oxides were low, rarely exceeding 2.0 wt. % (Table 1b), mean values of CaO (1.35 wt. %) was observed to be higher than average CaO (0.08 wt. %) of London's (2012) pegmatite.

TABLE 1A:

Major oxides (wt. %) composition of the tourmaline-bearing pegmatite compositions from Ijero-Ekiti

Samples / Major Oxides	R021	R022	R023	R024	R025	R026	R027	R05	R06	R07	R08	R09	R10
SiO_2	68.26	69.64	66.90	69.75	66.41	70.09	69.12	69.06	80.09	74.61	79.55	76.66	71.30
Al_2O_3	14.83	14.51	16.16	14.53	22.19	14.84	13.64	15.90	11.82	14.51	11.93	12.54	13.83
Fe_2O_3	3.91	2.91	3.81	2.94	1.82	2.14	4.33	2.53	0.83	1.15	0.77	1.80	3.19
MgO	1.24	1.01	1.05	1.01	0.66	0.76	1.51	0.66	0.03	0.17	0.03	0.32	0.84
CaO	2.27	1.73	2.23	1.77	1.30	1.37	2.55	1.42	0.04	0.35	0.04	0.67	1.77
Na_2O	3.15	3.23	3.12	3.27	2.34	3.25	3.08	3.26	4.42	5.16	4.38	3.95	3.21
K_2O	4.84	5.79	5.14	5.74	2.49	6.43	4.08	4.77	0.30	1.01	0.32	1.82	4.50
TiO_2	0.35	0.30	0.29	0.30	0.21	0.23	0.46	0.27	0.01	0.07	0.01	0.13	0.34
P_2O_5	0.31	0.10	0.55	0.09	0.17	0.13	0.08	0.09	0.17	0.21	0.16	0.14	0.09
MnO	0.10	0.05	0.15	0.05	0.22	0.04	0.07	0.06	0.05	0.04	0.04	0.05	0.05
Cr_2O_3	0.005	0.005	0.004	0.005	0.003	0.004	0.007	0.002	0.025	0.020	0.024	0.023	0.002
LOI	0.5	0.6	0.4	0.4	2.0	0.6	0.9	1.7	2.2	2.6	2.7	1.8	0.6
Sum	99.81	99.87	99.82	99.87	99.85	99.89	99.83	99.75	99.93	99.89	99.92	99.85	99.72
A/NK	1.86	1.61	1.96	1.61	4.59	1.53	1.91	1.98	2.50	2.35	2.54	2.17	1.79
A/CNK	1.45	1.35	1.54	1.35	3.62	1.34	1.40	1.68	2.48	2.23	2.52	1.95	1.46
Na/Na+Ca	0.59	0.66	0.59	0.66	0.65	0.71	0.56	0.70	0.99	0.94	0.99	0.86	0.65
Mg/Mg+Fe	0.21	0.23	0.19	0.23	0.24	0.23	0.23	0.18	0.03	0.11	0.03	0.13	0.19

TABLE 1B

Statistical summary of major oxide (wt. %) compositions of Ijero-Ekiti tourmaline-bearing pegmatites

Major Oxides	Range	Mean ± S.D
SiO_2	66.41 – 80.09	71.65 ± 4.59
Al_2O_3	11.82 – 22.19	14.71 ± 2.62
Fe_2O_3	0.77 – 4.33	2.47 ± 1.18
MgO	0.03 -1.51	0.71 ± 0.47
CaO	0.04 – 2.55	1.35 ± 0.84
Na_2O	2.34 – 5.16	3.52 ± 0.75
K_2O	0.30 – 6.43	3.63 ± 2.17
TiO_2	0.01 – 0.46	0.23 ± 0.14
P_2O_5	0.08 – 0.55	0.18 ± 0.13
MnO	0.04 – 0.22	0.07 ± 0.05
Cr_2O_3	0.00 – 0.03	0.01 ± 0.01

Dittrich *et al.* (2019) showed that low K_2O concentrations (0-4 wt. %) in LCT pegmatite reflect pegmatites dominated by a quartz and feldspar mineralogy, while high K_2O values (6-12 wt. %) support a mica dominated mineralogy. K_2O values ranging from 0.3 to 6.43 wt. % argue well for a quartz-feldspar with accessory mica mineralogy typical of LCT pegmatites (Bradley & McCauley, 2013). Total alkali concentrations which ranged from 4.70 to 9.68 wt. % supports the feldspar rich mineralogy. Grew (1996) demonstrated that in highly alkaline and/or silica- or aluminum-undersaturated conditions, tourmaline growth is inhibited and other borosilicates form instead. The fairly high concentrations of Na_2O in the pegmatites agree with the belief of Morgan & London (1989) that the solubility of aluminosilicates phases and components (e.g., Al) in borate fluids increases with increasing fluid alkalinity and may be indicative of changing speciation mechanisms in solution as a function of pH. Under ideal circumstances, uncontaminated B-rich, LCT-family melts should have considerable quantities of Na, allowing elbaite to precipitate, but magmas contaminated with Ca preferentially crystallise liddicoatite (Simmons, 2003; Brown & Wise, 2001; Selway *et al.*, 1998; Selway *et al.*, 1999). The low concentration of CaO (av. 1.35 wt. %) in the pegmatites stimulated tourmaline crystallisation, since high Ca concentrations, or high Ca/Al ratios, may not be favourable for tourmaline formation, and boron may be distributed in other species, such as danburite, serendibite, and axinite, to name a few (Frondel & Collette, 1957). MgO (av. 0.71 wt. %) is generally low in the analysed pegmatite samples since they have actually evolved from

LCT-family pegmatitic melts and so are not expected to have appreciable Mg, unless this element is introduced via contaminations from more mafic country rocks or other Mg-bearing rocks (Selway *et al.*, 2000; Tindle *et al.*, 2002). The Na/(Na+Ca) and Mg/(Mg+Fe) ratio (Table 1a) are low values and could favour late stage magmatic fluid differentiation which allows for the tourmaline mineralisation.

Deer *et al.* (1986) acknowledged the main controlling factor for colours in tourmalines to be the presence or absence of Fe. The varied Fe_2O_3 contents of the analysed pegmatites would have adverse effects on the chemical and physical properties, particularly the colours of the tourmaline minerals housed by the pegmatites. Tourmalines have been shown to capture a signature of their host's bulk composition, including elevated Li, where formed in pegmatites (Keller *et al.,* 1999, Selway *et al*, 1999, Hezel *et al*, 2011, London 2011). The chemical composition of tourmaline generally reflects the chemistry of the host rocks (Henry & Guidotti,1985; Demirel *et al.*,2009). Consequently, tourmaline crystals produced by the Ijero pegmatites were observed to vary widely in colours, consisting of red, pink, green, blue, yellow etc., mainly resulting from their diverse Fe content. Jimoh & Olatunji (2019) identified Fe as the primary chromophore controlling colour intensities in the southwestern Nigeria tourmalines. According to Brown & Wise (2001), Fe^{2+} or Fe^{3+} is the principle cause of green hues in elbaite.

The calculated ratios of the alumina saturation indices (ASI) for the sampled pegmatites are greater than one (A/CNK > 1, where $A = Al_2O_3$ and $CNK = CaO+Na_2O+K_2O$), indicating per-aluminous provenance for them. They therefore belong to the Lithium-Cesium-Tantalum (LCT) family pegmatites, since Černý (1985) found pegmatites of the LCT family to be of mild to extremely per-aluminous parent granitic compositions. The predominantly peraluminous nature of the Ijero pegmatites is also supported by the plot of Alumina Saturation Index (ASI) (A/CNK vs A/NK) (Fig. 7). The SiO_2 vs Total Alkali (Fig. 8) and the trilinear QAP (Fig. 9) plots describe the parent melt of these intrusive bodies as acidic in nature with granitic mineralogical composition. Major oxide geochemistry suggests that the Ijero pegmatites are granitic pegmatites with peraluminous character. Zen (1988) noted that such peraluminous rocks can be derived from sub-aluminous magma by factional crystallisation or by partial melting of peraluminous source rock.

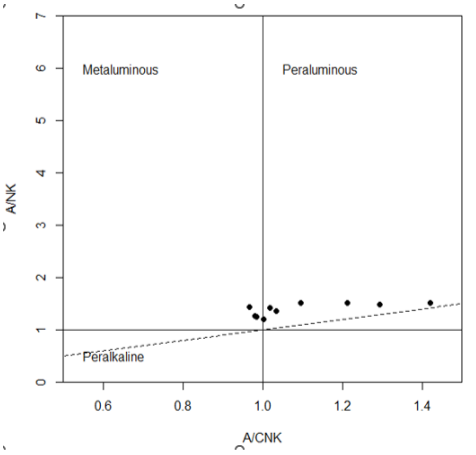

Fig. 7: Aluminum Saturation Index (ASI) in the plot of A/NK vs A/CNK describes a mainly peraluminous character for the samples of pegmatite from Ijero – Ekiti (Shand, 1943).

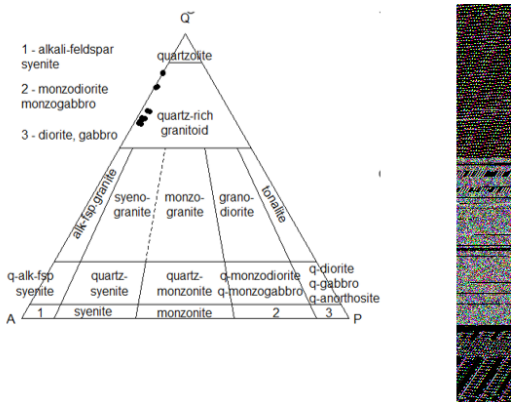

Fig. 8: The plot of Total Alkali vs Silica (TAS) has the samples plotted within the acid magma field indicating granitic composition (Cox *et al.*, 1979).

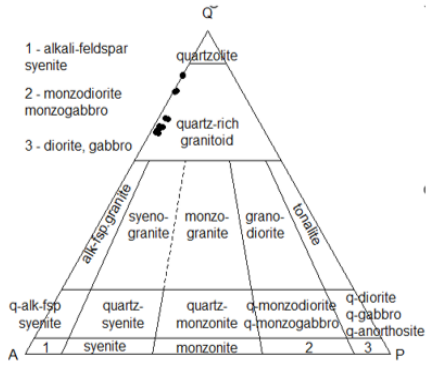

Fig. 9: The Ijero pegmatite fall well within the quartz-rich granitoid field on the QAP diagram (Streckeisen, 1976).

Turpin *et al.* (1990) pointed out that peraluminous granites are generally considered to be generated through partial melting of upper crustal rocks, especially during continent-continent collision events.

The inter-oxide associations existing among the major oxides of the Ijero-Ekiti tourmaline-bearing pegmatite samples, using Pearson correlation coefficients revealed some significant levels of positive and negative correlations (Table 2). While SiO_2 and Na_2O are positively correlated, they have both maintained negative correlations with all the other major oxides, and in most cases significant. All the analysed major oxides, except SiO_2 and Na_2O have however exhibited positive correlations among themselves. The negative correlations existing between SiO_2 and these major oxides confirm the credence of Kabata-Pendias (2001) that several interferences occur between Si^{4+} and other ions such as $Al^{3+,}$ Fe^{3+}, Mg^{2+}, Ca^{2+}, K^{+}, Ti^{4+} and Mn^{2+} in an environment, and these have adversely influenced the distributions of oxides of these ions in the Ijero-Ekiti pegmatite forming melt, maintaining inverse correlations. The negative correlation existing between SiO_2 and CaO (-0.86) is an indication of magmatic origin for the pegmatites (Frondel & Collette, 1957). The Harker plot of SiO_2 vs Na_2O (Fig. 10a) yielded a well-defined positive trend, while the plot of SiO_2 against Al_2O_3 (Fig. 10b) displayed a discernible negative trend, depicting an inverse relationship between them.

TABLE 2

Statistical correlation coefficients for major oxides of Ijero-Ekiti tourmaline-bearing pegmatite samples.

	SiO_2	Al_2O_3	Fe_2O_3	MgO	CaO	Na_2O	K_2O	TiO_2	P_2O_5	MnO
SiO_2	1									
Al_2O_3	-0.72**	1								
Fe_2O_3	-0.75**	0.15	1							
MgO	-0.82**	0.26	0.96**	1						
CaO	-0.86**	0.32	0.98**	0.99**	1					
Na_2O	0.83**	-0.65*	-0.66*	-0.74**	-0.77**	1				
K_2O	-0.78**	0.25	0.75**	0.80**	0.81**	-0.68**	1			
TiO_2	-0.82**	0.26	0.95**	0.97**	0.97**	-0.75**	0.80**	1		
P_2O_5	-0.22	0.18	0.23	0.10	0.19	-0.02	0.03	0.02	1	
MnO	-0.58*	0.86**	0.22	0.26	0.32	-0.61*	0.05	0.20	0.49	1

**. Correlation is significant at the 0.01 level (2-tailed) *. Correlation is significant at the 0.05 level (2-tailed)

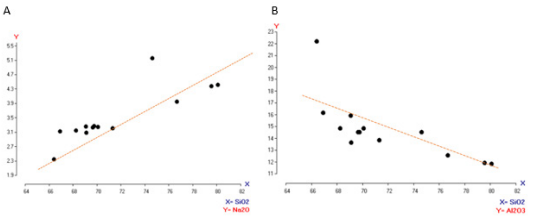

Fig. 10: Harker plot of A) SiO_2 vs NaO_2 and B) SiO_2 against Al_2O_3.

Pegmatites, being products of late-stage fluid-rich magma resulting from magmatic differentiation and fractional crystallisation, are rich in incompatible elements such as B, Be, F, P etc. The framework for the feldspar aluminosilicates accommodates K^+, Na^+, Ca^{2+}, Sr^{2+} and Ba^{2+} with Cs^+, Rb^+, Pb^{2+}, Tl^+ as impurities (Milovsky & Kononov, 1985), so also tourmaline, a boron aluminosilicate. The ability of tourmaline's crystal structure to accommodate major and trace elements of widely varying ionic charges and radii makes it an excellent monitor of the major and trace-element make-up of its local environment of growth (Jimoh, 2018). Trace element concentrations are presented in Table 3. Average values of trace element concentrations in the sampled pegmatites revealed enrichments in Cs (72.35 ppm), Rb (378.06 ppm), Be (4.19 ppm), Ta (4.73 ppm) and Sn (13.31 ppm) (Table 4) when compared to average Upper Continental Crust (UCC) values (Cs, 4.6 ppm; Rb, 112 ppm; Be, 3.0 ppm; Ta, 1.0 ppm and Sn, 5.5 ppm) of Taylor & McLennan (1995). The comparison to UCC values (Taylor & McLennan, 1995) (values in bracket) shows that these pegmatite bodies are depleted in Tl - 0.27 ppm (0.75 ppm), V - 24.15 ppm (97 ppm), W – 0.58 ppm (2.0 ppm) and Sr - 87.98 ppm (350 ppm). Niobium, Nb, (19.59 ppm) and Yttrium, Y, (33.11 ppm) are higher in concentration than the respective UCC values, 12 ppm and 22 ppm (Taylor & McLennan, 1995).

TABLE 3

Trace element composition (ppm) of the Ijero - Ekiti pegmatite.

Trace Elements (ppm)	R021	***R022***	***R023***	***R024***	***R025***	***R026***	***R027***	***R05***	***R06***	***R07***	***R08***	***R09***	***R10***
Ba	484	479	401	441	268	379	585	613	26	144	24	277	759
Be	3	4	4	2	12	1	0.5	5	6	5	7	4	0.5
Co	7.6	5.9	6.6	6.9	4.3	4.5	10.6	4.1	2.1	2.5	2.1	3.3	4.7
Cs	8.4	14.6	13.4	13.2	705.6	23	1.9	87.1	21.4	14	21.9	14.5	1.5
Ga	22.8	19	27.1	19.1	109.6	17.1	21.6	34.7	22.8	25.7	23.3	22	21.5
Hf	7.5	5.1	5.7	6.3	3.4	5.3	7.3	11.4	0.2	2.1	0.2	4.7	12.5
Nb	19.2	16.8	14.8	22.5	16.7	13.9	24.7	43.9	12.6	11.2	10.7	16.9	30.8
Rb	214.8	297.9	255.1	302.7	1427.1	397.4	131.1	1260	113.1	100.9	126.6	138.4	149.7
Sn	4	3	4	3	9	2	4	34	33	26	30	17	4
Sr	106.7	101.4	102	109.9	95.3	102.5	125.2	119.4	22.3	39.4	19.4	60	140.3
Ta	1	1	1.3	4.1	13.1	3.5	1.2	14	8.1	3.5	5.9	3.5	1.3
Th	31.8	15.6	15.4	15.7	11.9	16	22.9	25.9	0.1	6.3	0.1	12.1	40.8
U	14.3	2.6	5.9	3.2	3.1	5.8	4.7	8.1	3.3	5.7	3.1	4.4	8.2
V	36	31	31	31	21	25	51	22	11	11	4	13	27
W	0.3	0.3	0.3	0.3	0.7	0.3	0.3	2.5	0.7	0.3	0.3	0.9	0.3
Zr	224.1	138.1	145.8	170.6	87.7	141.1	212	272.1	3.8	61.9	3.3	141.6	356.3
Cu	12.4	13.9	9.6	16.6	14.4	9.2	22.4	9.5	3	4.7	2.6	7.1	21.1
Pb	8.1	10.1	10.6	10.1	12.4	10.8	4.5	4.2	1.9	2.7	1.7	3.7	4.6
Zn	48	42	38	44	25	30	61	72	8	21	7	38	90
Ni	4.8	4.6	3.9	4.2	2.6	3.4	6.4	1.9	5.3	4.2	4.7	5.2	2.3
As	0.3	0.3	0.3	0.5	1.6	0.3	0.3	0.3	1.8	1.5	1.5	1.4	0.6
Sb	0.1	0.1	0.1	0.1	0.2	0.1	0.1	0.1	0.1	0.2	0.2	0.1	0.1
Bi	0.6	0.3	1.1	0.3	2.8	0.4	0.1	0.2	0.6	0.6	0.6	0.7	0.1
Mo	0.9	0.7	0.5	0.6	0.4	0.6	1.1	1.9	1.7	1.6	1.6	2.2	0.7
Cd	0.2	0.05	0.4	0.05	0.05	0.05	0.05	0.05	0.05	0.05	0.05	0.05	0.05
Ag	0.1	0.1	0.1	0.1	0.1	0.1	0.1	0.1	0.1	0.1	0.1	<0.1	0.1
Au	0.5	0.3	0.9	0.03	0.9	0.7	1.3	0.3	0.3	0.3	0.3	0.3	0.3
Hg	0.01	0.01	0.01	0.01	0.01	0.01	0.01	0.01	0.01	0.01	0.01	0.01	0.01
Tl	0.2	0.2	0.2	0.2	0.7	0.1	0.3	0.3	0.3	0.2	0.2	0.3	0.3
Se	0.3	0.3	0.3	0.3	0.3	0.3	0.5	0.3	0.3	0.3	0.3	0.3	0.3
K/Rb	187.06	161.35	167.27	157.42	14.48	134.32	258.36	31.43	22.02	83.1	20.98	109.17	249.55
K/Cs	4783.3	3292.21	3184.35	3609.94	29.3	2320.84	17826.59	454.63	116.38	598.9	121.3		24904.8
Rb/Cs	25.57	20.4	19.04	22.93	2.02	17.28	69	14.47	5.29	7.21	5.78	9.54	99.8
Be/Ta	3	4	3.08	0.49	0.92	0.29	0.42	0.36	0.74	1.43	1.19	1.14	0.38
Nb/Ta	19.2	16.8	11.38	5.49	1.27	3.97	20.58	3.14	1.56	3.2	1.81	4.83	23.69
Y	53.4	32.4	34.1	38.2	23.8	31.5	50.9	53.1	0.9	12.7	1	25.8	72.6
La	66.9	39.4	41.5	37	20.6	43.8	49.6	67.1	1	17	1	30.9	101.2
Ce	130	77.5	80.3	70.8	43	84.6	97.6	129	1.7	31.5	1.6	61.8	199.5
Pr	13.69	7.99	8.64	7.49	4.42	8.41	11.04	14.37	0.22	3.61	0.23	6.99	22.93
Nd	52	29.1	30.9	27.3	16.6	27.9	40	51.5	1	12.2	0.9	24.1	81.7
Sm	8.98	5.3	5.82	5.02	3.18	4.73	7.93	10	0.26	2.46	0.2	4.77	16.13
Eu	0.75	0.58	0.54	0.55	0.38	0.41	0.86	0.86	0.03	0.21	0.03	0.39	1.08
Gd	8.56	5.16	5.93	5.54	3.53	4.53	7.77	9.43	0.25	2.3	0.2	4.54	15.06
Tb	1.36	0.89	0.93	0.97	0.61	0.79	1.35	1.47	0.04	0.38	0.04	0.72	2.21
Dy	7.97	5.72	5.72	5.73	3.89	5.21	7.97	8.91	0.22	2.17	0.22	4.46	12.31
Ho	1.72	1.17	1.27	1.3	0.89	1.11	1.7	1.71	0.03	0.41	0.02	0.81	2.32
Er	5.08	3.78	3.65	4.1	2.59	3.5	5.66	4.88	0.08	1.22	0.08	2.45	6.74
Tm	0.73	0.59	0.56	0.61	0.38	0.51	0.8	0.74	0.02	0.18	0.02	0.37	1.01
Yb	5.17	3.75	3.47	3.95	2.18	3.42	5.37	4.65	0.09	1.16	0.1	2.32	6.4
Lu	0.75	0.6	0.54	0.6	0.33	0.55	0.82	0.67	0.02	0.17	0.02	0.34	0.93

TABLE 4

Statistical summary of trace element compositions of Ijero-Ekiti tourmaline-bearing pegmatites

Trace elements	*Range (%)*	*Mean ± S. D.*
Sc	0.50 – 8.00	4.08 ± 2.46
Ba	24.00 – 759.00	375.38 ± 222.74
Be	0.50 – 12.00	4.19 ± 3.08
Co	2.10 – 10.60	5.02 ± 2.46
Cs	1.50 – 705.60	72.35 ± 191.47
Ga	17.10 – 109.60	29.72 ± 24.40
Hf	0.20 – 12.50	5.52 ± 3.70
Nb	10.70 – 43.90	19.59 ± 9.26
Rb	100.90 – 1427.10	378.06 ± 439.07
Sn	2.00 – 34.00	13.31 ± 12.83
Sr	19.40 – 140.30	87.98 ± 39.52
Ta	1.00 – 14.00	4.73 ± 4.45
Th	0.10 – 40.80	16.51 ± 11.69
U	2.60 – 14.30	5.57 ± 3.21
V	4.00 – 51.00	24.15 ± 12.59
W	0.30 – 2.50	0.58 ± 0.61
Zr	3.30 – 356.30	150.65 ± 100.86
Y	0.90 – 72.60	33.11 ± 21.10
Mo	0.40 – 2.20	1.12 ± 0.61
Cu	2.60 – 22.40	11.27 ± 6.33
Pb	1.70 – 12.40	6.57 ± 3.85
Zn	7.00 – 90.00	40.31 ± 23.90
Ni	1.90 – 6.40	4.12 ± 1.29
As	0.30 – 1.80	0.82 ± 0.62
Cd	0.10 – 0.40	0.13 ± 0.09
Sb	0.10 – 0.20	0.12 ± 0.04
Bi	0.10 – 2.80	0.65 ± 0.70
Au	0.30 – 1.30	0.52 ± 0.33
Tl	0.10 – 0.70	0.27 ± 0.14
Se	0.30 – 0.50	0.32 ± 0.06

Černý (1992) gave a pegmatite classification based on rare metal enrichment: LCT pegmatites with Li, Rb, Cs, Be, Ga, Sn, Ta > Nb (B, P, F); NYF pegmatites with Nb > Ta, Ti, Y, REE, Zr, Th, U(F); and pegmatites with a mixed geochemical signature. Using the classification scheme of Ginsburg *et al.* (1979) and revised by Černý (1992), the studied pegmatite bodies based on their trace element concentrations (Li, Rb, Cs, Be, Ga, Y, REE, Sn, Ti, U, Th, Hf, Nb, Ta) are categorised as rare element pegmatites. Rare element class pegmatites are believed to be derived from magmatogenic processes. This implies that trace element mobility can be a major tool in determining the nature and origin of this class of pegmatites. The aluminum saturation index (ASI) and the rare metal composition of Rb, Cs, Be, Ga, Sn, Ta > Nb supports an LCT type pegmatite for the Ijero pegmatite despite having an average Nb concentration greater than the UCC value of Taylor & McLennan (1995). Černý (1992) argued for Niobium – Yttrium – Fluorine (NYF) pegmatite with A-type granitic parentage whenever geochemical data suggests metaluminous character. The TAS plot (Fig. 8) presents a dominant subalkaline melt parentage for the Ijero pegmatite which supports the argument for LCT type pegmatite and does not support a NYF type despite that most samples recorded Nb concentrations above UCC Nb value of Taylor & McLennan (1995).

The spider plot (Fig 11), using concentrations of Taylor & McLennan (1995) as normalising values, with evidence for enrichments in Cs, Th, U and Ta, while Nb is markedly depleted favours LCT pegmatite class. This plot suggests that the pegmatites are fractionated, with Cs, Th and Ta concentrated in late mineral phases such as albite and micas. Anatexis of undepleted upper- to

middle-crustal protoliths - supracrustal and/or basement, undergoing their first melting event - is the major geologic process responsible for the generation of fertile melts that yield post-orogenic LCT pegmatites (Černý, 1990, 1991a). Fractionation trend suggestive of two potential mineralisations (the muscovite class and the rare metal class) is observed in the K/Rb vs K/Cs plot (Fig. 12b). The Sr values which fell within Černý's (1992) range of 10 – 100 ppm suggest mineralisation (Fig. 12a). Figure 12b illustrates that the samples fall within the margins of the mineralised rare metal (Be, Ta > Nb) to non mineralised muscovite pegmatites similar to the Cross Lake field in Manitoba (Černý, 1992).

Rare earth element (REE) concentrations, when normalised using chondrite values (Boynton, 1984) suggest feldspar fractionation with a negative europium (Eu^{3+}) anomaly from pegmatites with upper continental crust origin. Generally, the samples display light REE (LREE)-enriched and heavy REE (HREE)-depleted patterns (Fig. 13), suggesting upper continental crust sourced material. The REE patterns for the analysed pegmatite samples generally exhibit fractionated asymmetric concave-upward shapes, with strong negative Eu anomalies, an indication for granite-related pegmatites.

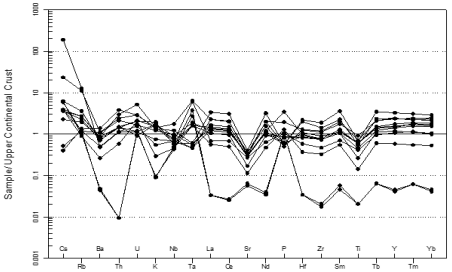

Fig. 11:Cs, Th and Ta enrichment is observed from the spider plot normalised using values from Taylor & McLennan (1995).

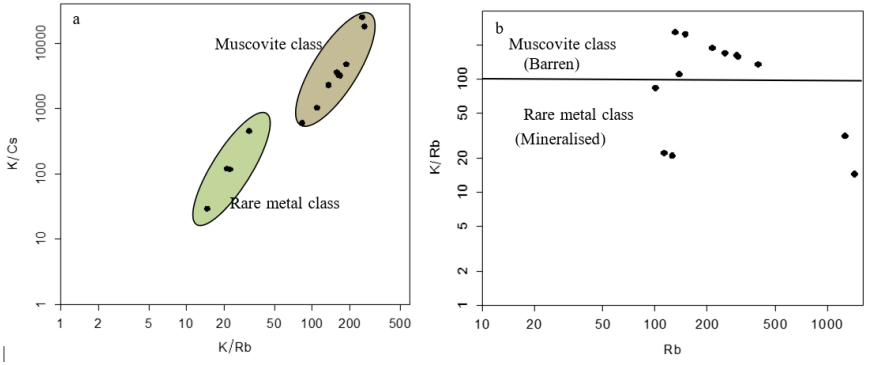

Fig. 12: a) Fractionation trend from K/Rb vs K/Cs demonstrated change in mineralisation trend. b) Plot of Rb vs K/Rb discriminated the mineralisation of the pegmatites (modified after Stavrov *et al*. 1969).

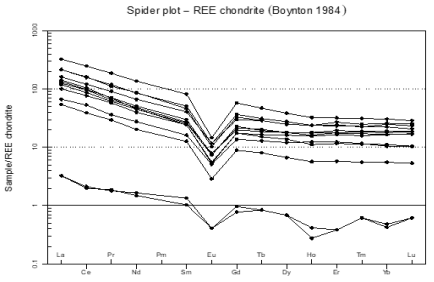

Fig. 13:Rare earth element (REE) normalised plot (Boynton, 1984) revealed negative Eu anomaly which supports feldspar fractionation.

Geophysical characterisation

The existence of lithologic interfaces or geo-electric boundaries within the subsurface is as a result of variations in ground resistivity that exist across each lithofacies. The inversion of the electrical resistivity sounding data gives rise to 2D geoelectric parameters in form of resistivity and thickness which were used to delineate the mineralised layers. Typical geoelectric curves from the study are shown in figure 14 which correspond to iterated VES data in the area. Relatively low root mean square (RMS) errors were recorded for all the output models produced. The few presented sounding curves represented many generated from the study area. 3 to 5-layer models were obtained across the entire study area. H-type and AHA-type covered 40 and 20% of the total study area respectively, while A, HA, KQ and AAK covered 10% of the area (as presented in Table 5). Categorisation of a sounding curve is based on its resistivity values (Adagunodo *et al.*, 2018). A 3-layer case consist ℓ_1, ℓ_2 and ℓ_3 of which are grouped into four types namely: A, H, K, and Q (Adagunodo *et al*., 2018, Sunmonu *et al.*, 2015). HA, KQ, AAK, AHA shown in Table 5 are few among many 4 and 5- layer models that can be produced (Ologe & Ola-Buraimo, 2022; Sunmonu *et al*., 2015). The interpretation of electrical soundings gives geological inference that correlate to the resistivity data and the geological settings of the area of study (Loke, 1999). The study area showed three to five layers lithology (Table 6) which comprised topsoil, basement (fractured or fresh basement) to topsoil, laterite and basement (fractured or fresh basement). From Table 6, topsoil which is mainly superficial layer has resistivity values ranging between 183-1030 Ohm-m and maximum thickness of 1.3 m. This layer is believed to have little or no mineralogical significance because of its thin thickness. Below the lateritic zone is the anomalous layer which is characterised by high resistivity value ranging between 1086-9489 Ohm-m with surface to maximum depth of the layer to be 20.8 m which affirms the tourmaline-rich pegmatite while areas with low resistivity values are suggestive to aid mine design and exploitation of the minerals. In some cases, the subsurface with weathered portion also have low values of resistivity which could be attributed to presence of groundwater.

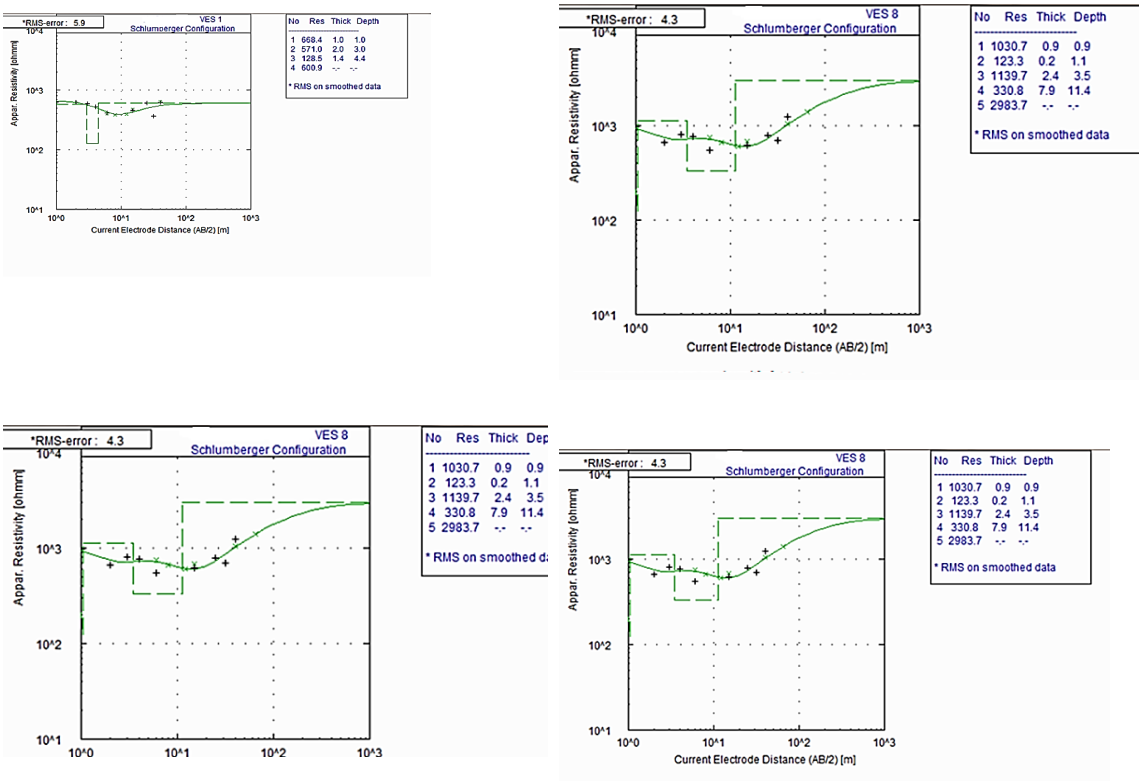

Fig. 14: Typical VES curves from the study area.

TABLE 5

Sounding Curves Classification

Type of Curves	***Resistivity Model***	***Number of Stations***	***Curve Type Percentage %***
H	$\ell_1>\ell_2<\ell_3$	04	40
A	$\ell_1<\ell_2<\ell_3$	01	10
HA	$\ell_1>\ell_2>\ell_3<\ell_4$	01	10
KQ	$\ell_1>\ell_2<\ell_3>\ell_4$	01	10
AAK	$\ell_1<\ell_2<\ell_3>\ell_4<\ell_5$	01	10
AHA	$\ell_1>\ell_2<\ell_3>\ell_4<\ell_5$	02	20
Total		10	

TABLE 6

Electrical Resistivity Parameters of the Study Area

VES No	*No of layers*	*Resistivity Range (Ωm)*	*Thickness (m)*	*Depth (m)*	*Resistivity Model*	*Lithology*
	1		1	1		Topsoil
1	2	128.5-668.4	2	3	$\ell_1>\ell_2>\ell_3<\ell_4$	Laterite
	3		1.4	4.4		Fractured basement
	4		-	-		Fresh basement
	1		0.4	0.4		Topsoil
2	2	415.3-1447.6	3.1	3.5	$\ell_1>\ell_2<\ell_3$	Fractured basement
	3		-	-		Fresh basement
	1		0.3	0.3		
3	2	188.6-1590	1.6	1.9	$\ell_1>\ell_2<\ell_3>\ell_4$	Topsoil
	3		7	7		Laterite
	4		-	-		Fractured basement
						Fresh basement
	1		1.3	1.3		Topsoil
	2		6.6	7.9		Laterite
4	3	208.4-4392.7	7.8	15.7	$\ell_1<\ell_2<\ell_3>\ell_4<\ell_5$	Fractured basement
	4		5.1	20.8		Fresh basement
	5		-	-		
	1		0.9	0.9		Topsoil
5	2	236.3-1140.1	6.5	7.4	$\ell_1>\ell_2<\ell_3$	Fractured basement
	3		-	-		Fresh basement
	1		0.7	0.7		Topsoil
	2		0.5	1.2		Laterite
6	3	168.6-9489.4	5.9	7.1	$\ell_1>\ell_2<\ell_3>\ell_4<\ell_5$	Fractured basement
	4		4.7	11.8		Fresh basement
	5		-	-		
	1		0.4	0.4		Topsoil
7	2	286.5-1957.7	9.7	10.1	$\ell_1>\ell_2<\ell_3$	Fractured basement
	3		-	-		Fresh basement
	1		0.9	0.9		Topsoil
	2		0.2	1.1		Laterite
8	3	123.3-2983.7	2.4	3.5	$\ell_1>\ell_2<\ell_3>\ell_4<\ell_5$	Fractured basement
	4		7.9	11.4		Fresh basement
	5		-	-		
	1		0.7	0.7		Topsoil
9	2	342.5-1850.7	0.9	1.6	$\ell_1>\ell_2<\ell_3$	Fractured basement
	3		-	-		Fresh basement
10	1		0.8	0.8		Topsoil
		290.3-1424.2	1.4	2.2	$\ell_1<\ell_2<\ell_3$	Fractured basement
			-	-		Fresh basement

Conclusion

Geological field observation showed Ijero-Ekiti tourmaline-bearing pegmatites to be mineralised, with occasional occurrences of gem tourmaline crystals found in associations with other gem, metallic and rock forming minerals either in miarolitic cavities within the granitic pegmatites, and in veins along contacts with their host rocks or are scattered within the pegmatitic bodies. The aluminum saturation index (ASI) and the rare metal composition of Rb, Cs, Be, Ga, Sn, Ta > Nb supports an LCT type rare elements pegmatite for the studied pegmatite bodies despite having an average Nb concentration greater than the UCC value of Taylor & McLennan (1995). Some of these pegmatites are seen to be enriched in B-metasomatism hence the abundance of tourmaline, suggesting that they emanated from highly mineralised magma and are believed to represent late-stage pneumatolytic fluids derived from acidic magma bodies. The K/Cs vs K/Rb and Rb vs K/Rb plots suggested mineralisations that yielded a muscovite pegmatite class and a rare metal pegmatite class. Matheis (1987) argued that rare-metal pegmatites of Nigeria are products of high-grade metamorphic conditions, which were emplaced along a deep-seated continental lineament and enhanced by high crustal heat flow and the addition of fluid phases. There is therefore the possibility that the gem-bearing pegmatites from the study area were derived from the anatexis of un-depleted upper to middle crustal materials. Data for the vertical electric sounding (VES) reveals a lateritic subsurface that is possibly mineralised. The data recorded high resistivity values for this anomalous layer to a depth of 20.8 m.

References

ADAGUNODO, T. A., AKINLOYE, M. K., SUNMONU, L. A., AIZEBEOKHAI , A. P., OYEYEMI, K. D. & ABODUNRIN, F. O. (2018). Groundwater Exploration in Aaba Residential Area of Akure, Nigeria. *Front. Earth Sci.,* **6**, 66. doi: 10.3389/ feart.2018.00066.

ADETUNJI, A. & OCAN, O. O. (2010). Characterisation and Mineralization Potentials of Granitic Pegmatites of Komu area, Southwestern Nigeria. *Resource Geology*, **60** (1), 87–97.

ADETUNJI, A., OLAREWAJU, V. O., OCAN, O. O., MACHEVA, L. & GANEV, V. Y. (2018). Geochemistry and U-Pb zircon geochronology of Iwo quartz potassic syenite, southwestern Nigeria: Constraints on petrogenesis, timing of deformation and terrane amalgamation, *Precambrian Research*, doi: https://doi. org/10.1016/ j.precamres.2018.01.015.

AMIGUN, J. O. & ANU, A. L. (2013). Integrated Geophysical Mapping of Structures beneath Ijero – Aramoko Area, Southwestern Nigeria: Implications for Control of Mineralisation, *Acta Geologica Sinica,* **87**, 708.

BLACK, R. (1980). Precambrian of West Africa, *Episodes*, **4**, 3-8.

BOYNTON, W. V. (1984). Geochemistry of the rare earth elements: meteorite studies. In: P. Henderson (ed), *Rare Earth Element geochemistry, Elsevier,* p. 63 – 114.

BRADLEY, D. & MCCAULEY, A. (2013). A preliminary deposit model for lithium-cesium-tantalum (LCT) pegmatites (ver. 1.1, December 2016): *U.S. Geological Survey Open-File Report,* 7, p. 2013–1008, https:// doi.org/10.3133/ofr20131008.

BRADLEY, D. C., MCCAULEY, A. D. & STILLINGS, L. L. (2017). Mineral-deposit model for lithium-cesium-tantalum pegmatites: *United States Geological Survey,*

Reston, VA, Scientific Investigations Report ***2010-5070***, 58.

BROWN, C. D. & WISE, M. A. (2001). Internal zonation and chemical evolution of the Black Mountain granitic pegmatite, Maine. *Can. Mineral*. **39**, 45-55.

ČERNÝ, P., MEINTZER, R. E. & ANDERSON, A. J. (1985). Extreme fractionation in rare-element granitic pegmatites: selected examples of data and mechanisms. *Can. Mineral.* **23**, 381-421.

ČERNÝ, P. (1989a). Characteristics of pegmatite deposits of tantalum. In Lanthanides, Tantalum and Niobium (eds P. Moller, P. Černý and F. Saupe), *Soc. Geol. Appi. Ore Deposits Spec. Publ.,* **7**, 192-236.

ČERNÝ, P. (1990). Distribution, affiliation and derivation of rare-element granitic pegmatites in the Canadian Shield. *Geol. Rundschau,* **79**, 183-226.

ČERNÝ, P. (1991a). Fertile granites of Precambrian rare element pegmatite fields: is geochemistry controlled by tectonic setting or source lithologies? *Precambr. Res.*, **1**, 429–468.

ČERNÝ, P. (1991b). Rare-element granitic pegmatites. Part 2: regional to global environments and petrogenesis. *Geosci. Can.,* **18**, 68–81.

ČERNÝ, P. (1992). Geochemical and petrogenetic features of mineralisation in rare-element granitic pegmatites in the light of current research. *Applied Geochemistry,* **7** (5), 393–416. doi:10.1016/0883-2927(92)90002-k.

COX, K. G., BELL, J. D. & PANKHURST, R. J. (1979). The interpretation of igneous rocks. *George Allen and Unwin*., p. 450. http://dx.doi.org/10.1007/978-94-017-3373-1.

DEMIREL, S., GONCUOGLU, M. C., TOPUZ, G. & ISIK, V. (2009). Geology and chemical variations in tourmaline from the quartz-tourmaline breccias within the Kerkenez granite-monzonite massif, Central Anatolian Crystalline Complex, Turkey. *The Canadian Mineralogist,* **47** (4), 787–799.

DEER, W. A., HOWIE, R. A. & ZUSSMAN, J. (1986). Rock Forming Minerals-Disilicates and Ring Silicates (2nd edition). *Longmans, Green and Co. Ltd. 1B*, p. 559–602.

DENTITH, M. & MUDGE, S. T. (2014). Geophysics for the Mineral Exploration Geoscientist. *Cambridge: Cambridge University Press*. p. 454.

DITTRICH, T., SEIFERT, T., SCHULZ, B., HAGEMANN, S., GERDES, A. & PFÄNDER, J. (2019). Geochemistry of LCT Pegmatites. *Computational Methods for Single-Cell Data Analysis,* p. 77–86. doi:10.1007/978-3-030-10943-1-4.

DUURING, P. (2020). Rare-element pegmatites: a mineral systems analysis: *Geological Survey of Western Australia, Record*, 2020, **7**, 6.

ELATIKPO, S. M., DANBATTA, U. A. & NAJIME, T. (2013). Geochemistry and Petrogenesis of Gneisses Around Kafur-Yari Bori-Tsiga area within the Malumfashi Schist Belt, Northwestern, Nigeria. *Journal of Environment and Earth Science,* **3** (7), 171-180.

ELUEZE, A. A. (1992). Rift system for Proterozoic schist belts in Nigeria. *Tectonophysics,* **209**, 167–169.

ELUEZE, A. A. (2002). Compositional Character: A veritable tool in the appraisal of geo-materials. *An inaugural lecture*. *University of Ibadan*, p. 43.

FRONDEL, C., & COLLETTE, R. L. (1957). Synthesis of tourmaline by reaction of mineral grains with NaCl-H3BO3 solution, and its implications in rock metamorphism. *American Mineralogist,* **42**, 754–758.

GARBA, I. (2003). Geochemical discrimination of newly discovered rare-metal bearing and barren pegmatites in the Pan-African

(600±150Ma) basement of northern Nigeria. *Applied Earth Science (Trans. Inst. Min. Metall.),* **112**, 287–292.

GINSBURG, A. I., TIMOFEYEV I. N. & FELDMAN L. G. (1979). Principles of Geology of the Granitic Pegmatites. *Nedra, Moscow,* p. 296.

GRANT, N. K. (1970). The geochronology of Precambrian basement rocks from Ibadan, South-Western Nigeria. *Earth Planet Sci Lett.,* **10**, 29–38

GREW, E. S. (1996). Borosilicates (exclusive of tourmaline) and boron in rock-forming minerals in metamorphic environments. *Reviews in Mineralogy,* **33**, 387–502.

HARPER, C. T., SHERRER. G., MCCURRY, P. & WRIGHT, J. B. (1973). K. Ar retention ages from the Pan- African of Northern Nigerian, *Bull. Geol. Soc. Amer.*, p. 919–926.

HAWTHORNE, F. C., MCDONALD, D. J. & BURNS, P.C. (1993). Reassignment of cation site occupancies in tourmaline: AI-Mg disorder in the crystal structure of dravite. *American Mineralogist*, **78**, 265–270.

HENRY, D. J. & GUIDOTTI, C. V. (1985). Tourmaline as a petrogenetic indicator mineral: an example from the staurolite-grade metapelites of NW Maine. *American mineralogist*. **70**, 1–15.

HEZEL, D. C., KALT, A., MARSCHALL, H. R., LUDWIG, T. & MEYER, H.-P. (2011). Major element and Li, Be compositional evolution of tourmaline in an S-type granite–pegmatite system and its country rocks: an example from the island of Ikaria, Aegean Sea, Greece. *Can. Mineral.,* p. 49.

JIMOH, R. O. (2018). Geochemical characterisation of tourmaline and beryl from selected gem-bearing pegmatites in southwestern Nigeria. *Unpubl. PhD thesis*, University of Ibadan.

JIMOH, R. O. & OLATUNJI, A. S. (2019). Iron: A significant determinant of colours in gem tourmalines from southwestern Nigeria. *Nigerian Journal of Pure and Applied Sciences (NJPAS),* **32** (2), 3447–3460. ISSN 0794-0378.

KABATA-PENDIAS, A. (2001). Trace elements in soils and plants. 3rd ed. CRS press. NY.

KEAREY, P., MICHAEL, B. & IAN, H. (2002). An Introduction to Geophysical Exploration. *London: Blackwell Science Limited*, p. 243–454.

KELLER, P., ROBLES, E. R., PÉREZ, A. P. & FONTAN, F. (1999). Chemistry, paragenesis and significance of tourmaline in pegmatites of the southern tin belt, central Namibia: *Chemical Geology*, **158**, 203–225.

KINNAIRD, J. A. (1984). Contrasting styles of Sn-Nb-Ta-Zn mineralisation in Nigeria. *J. Afr. Ear. Sci.*, **2** (2), 81–90.

LOKE, M. H. (1999). A Practical Guide to 2D and 3D Surveys. Electrical Imaging Surveys for Environmental and Engineering Studies, p. 8-10.

LONDON, D. (1996). Granitic pegmatites. *Transactions of the Royal Society of Edinburgh: Earth Sciences,* **87**, 305-319.

LONDON, D. (2011). Experimental synthesis and stability of tourmaline: a historical perspective. *Can. Mineral.* **49**, 117–136.

LONDON, D., MORGAN VI, G. B., PAUL, K. A. & GUTTERY, B. M. (2012). Internal Evolution of Miarolitic Granitic Pegmatites at the Little Three Mine, Ramona, California, USA. *The Canadian Mineralogist,* **50** (4), 1025–1054. doi:10.3749/canmin.50.4.1025.

LONDON, D. (2018). Ore-forming processes within granitic pegmatites. *Ore Geology Reviews.* **101**, 349–383.

MATHEIS, G. (1987). Nigerian rare metal pegmatites and their lithological framework. *J. Geol*., **22** (52), 271–291. doi:10.1002/gj.3350220620.

MILOVSKY, A. V. & KONONOV, O. V. (1985). Mineralogy. *Mir Publishers, Moscow,* p. 320.

MORGAN, G. B., & LONDON, D. (1989). Experimental reactions of amphibolite with boron-bearing aqueous fluids at 200 MPa: implications for tourmaline stability and partial melting in mafic rocks. *Contributions to Mineralogy and Petrology*, **102**, 281–297.

MOSURO, G., BAYEWU, O. & OLORUNTOLA, M. (2011). Geophysical investigation for groundwater exploration in Kobape via Abeokuta SW, Nigeria. https:// doi. org/ 10. 13140/2. 1. 4183. 1686.

OKUNLOLA, O. A. & OYEDOKUN, M. O. (2009). Compositional trends in rare metal (Ta-Nb) mineralisation potential of pegmatite and associated lithologies of Igbetti area, southwestern Nigeria. *Journal of the Faculty of Science, University of Ibadan*, **8** (2), 114–127.

OLATUNJI, A. S. & JIMOH, R. O. (2017). Major Oxides Geochemistry of Some Tourmalines from Southwestern Nigeria. *Minna J. Geosci. (MJG),* **1**(1), 41–64.

OLISA, O. G., OKUNLOLA, O. A. & OMITOGUN, A. A. (2018). Rare Metals (Ta-Nb-Sn) Mineralization Potential of Pegmatites of Igangan Area, Southwestern Nigeria. *Journal of Geoscience and Environment Protection,* **6**, 67-88.

OLOGE, O. & OLA-BURAIMO, A. O. (2022). Evaluation of aquifer characteristics within Birnin Kebbi metropolis, Northwestern Nigeria using geoelectric survey. *Jordan Journal of Earth and Environmental Sciences,* **13** (1), 60–63.

OYINLOYE, O.A. (2011) Geology and Geotectonic Setting of the Basement Complex Rocks in South Western Nigeria: Implications on Provenance and Evolution, *Earth and Environmental Sciences*. doi:10.5772/26990.

RAHAMAN, M. A., AJAYI, T. R., OSHIN, I. O., & ASUBIOJO, F. O. (1988). Trace elements Geochemistry and geotectonic setting of Ife-Ilesha schist belts. *Precambrian Geology of Nigeria*, *GNS Publications. Kaduna*, 241–256.

RAHAMAN, M. A. & OCAN O. (1978). On relationships in the Precambrian migmatite-gneisses of Nigeria. *Nig. J. Min. Geo*l., **15**, 23–32.

SELWAY, J. B., NOVÁK, M., HAWTHORNE, F.C., ČERNÝ, P., OTTOLINI, L. & KYSER, T.K. (1998). Rossmanite,

Received 24 Feb 24; revised 30 Jul 24.